7 Manipulation of Trailing-Edge Vortices

In this chapter, an attempt at eliminating certain negative aspects of the dynamic-stall process by careful tuning of the airfoil kinematics has been performed. A so-called quick-pitch motion around the bottom of the stroke is used to counteract the development of a TEV. The timing of these kinematics are varied and evaluated in comparison to the pure-plunge reference case.

7.1 Parameter Space

The reduced frequency was chosen such that a distinct vortical wake was formed for the given amplitude ($h_0/c = 0.5$) and mean angle of attack ($\alpha_0 = 8°$). The appearance of such a distinct mushroom-wake structure in this facility was first observed at $k > 0.2$, as reported in section 5.2.2. A pure-plunge sinusoidal motion used to augment lift has inherent disadvantages, as described in section 6.3.1. These include among others the formation of a TEV, which diminishes lift on the airfoil. Another disadvantage is the long recovery period, from $t/T = 0.333$ up until the middle of the upstroke, where the region over the airfoil remains separated for a prolonged period of time. While the flow is fully-separated, lift drops and the pitch-down moment and drag are increased, see Carr et al (1977). In order to improve performance various kinematics such as a so-called *peak-shifted* case have been tested in section 6.3.1. While they offer some benefits in terms of LEV formation, more radical alterations of the airfoil kinematics could further improve the performance of the plunging airfoil, specifically by targeting the most disadvantageous aspects of the flow and minimizing them. In this study some of the detrimental aspects of dynamic stall have been reduced by superimposing a quick-pitch motion, which counteracts the TEV and the lingering separation. In Fig. 7.1 the breakdown of the pure-plunge and quick-pitch motions is presented.

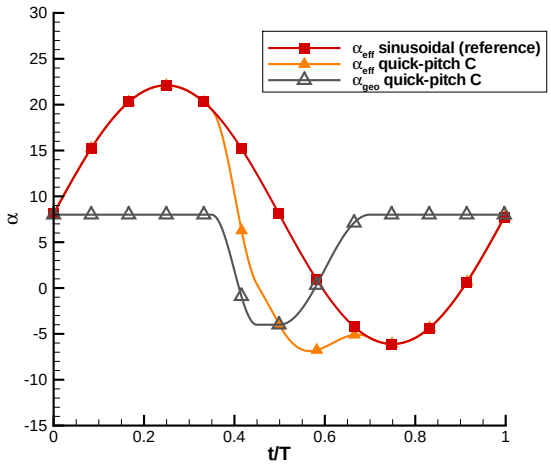

Figure 7.1: Individual components of the quick-pitch motion: effective angle of attack (α_{eff}) for the sinusoidal-plunge and quick-pitch cases, geometric angle (α_{geo}) of attack for the quick-pitch case.

The effective angle-of-attack distribution as a function of period for all quick-pitch cases is presented in Fig. 7.2. The quick-pitch kinematics are based upon the sinusoidal motion of the reference case. At a varying time towards the end of the downstroke, a pitch-down motion (pronation) is superimposed onto the reference case. The quick-pitch motion begins by sinusoidally pitching the airfoil down at a frequency five times greater than that of the plunging motion itself. This is followed by a pause in the pitched-down position. Thereafter the airfoil returns to its initial geometric angle of attack at half the rate of the pronation. The timing for the pause and the pitch-up motion were chosen in a way as to maintain as smooth a motion as possible at the bottom-dead-center position, so as to facilitate flow reattachment. The following equation describes the effective angle-of-attack distribution for the pure-plunge motion:

$$\alpha_{plunge}(t) = \alpha_0 + \arctan\left(\frac{2\pi f h_o \sin(2\pi f t)}{U_\infty}\right). \tag{7.1}$$

As an example Eq. 7.2 describes the superposition of the quick-pitch motion on top of the pure-plunge motion for the quick-pitch C case:

$$\alpha_{eff}(t) = \begin{cases} \alpha_{plunge}(t), & \text{for } 0 \leq t/T < 0.35 \\ \alpha_{plunge}(t) - \alpha_1 \left(\cos\left(2n\pi t + \pi\right) + 1\right), & \text{for } 0.35 \leq t/T < 0.45 \\ \alpha_{plunge}(t) - \alpha_1, & \text{for } 0.45 \leq t/T < 0.5 \\ \alpha_{plunge}(t) - \alpha_1 \left(\cos\left(n\pi t + \pi\right)\right), & \text{for } 0.5 \leq t/T < 0.7 \\ \alpha_{plunge}(t), & \text{for } 0.7 \leq t/T < 1 \end{cases} \tag{7.2}$$

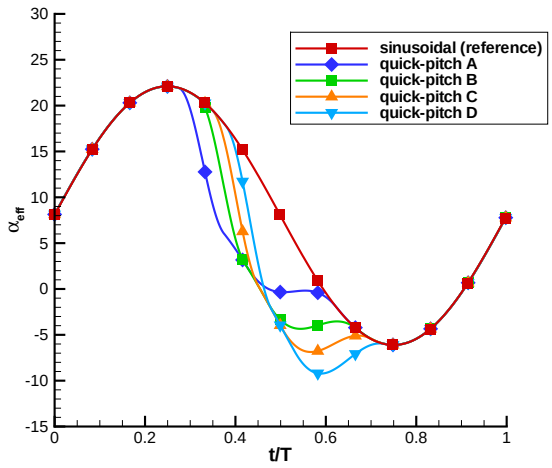

Figure 7.2: Effective angle-of-attack distribution for the various quick-pitch cases; note symbols represent the 12 measurement phases over the period.

The goal of the quick-pitch kinematics was to specifically target the TEV and the fully-separated flow over the airfoil after the LEV has pinched-off. A fast pitching motion is necessary in order to respond to the TEV quickly without affecting the LEV formation process. Furthermore, by pitching down quickly the local effective angle of attack at the trailing edge is reduced (known as dynamic cambering), which further combats the development of the TEV.

The only difference between the various quick-pitch cases is the timing of the beginning of the pitching motion. The pronation (pitch-down) and following supination

(pitch-up) are the same for all cases. The timing of the pronation is important as it dictates when the effective angle of attack drops below the static-stall angle, and therefore when production of vorticity at the leading edge is significantly reduced. The timing of the pronation (t_{pro}/T), as well as the resulting timing in crossing back down below the static-stall angle ($t_{<stall}/T$), the end of the supination (t_{sup}/T) and the pause duration (t_{pause}/T), can be found in Table 7.1.

Table 7.1: Characteristic timing of kinematics and the crossing of the static-stall angle for the various quick-pitch cases.

case	t_{pro}/T	f_{pro} (Hz)	t_{pause}/T	f_{sup} (Hz)	t_{sup}/T	$t_{<stall}/T$
reference	–	–	–	–	–	0.476
quick-pitch A	0.275	12.5	50	6.25	0.625	0.342
quick-pitch B	0.320	12.5	50	6.25	0.670	0.376
quick-pitch C	0.350	12.5	50	6.25	0.7	0.398
quick-pitch D	0.380	12.5	50	6.25	0.73	0.419

7.2 Results

7.2.1 Vorticity

In this section the vorticity distributions of the quick-pitch cases are compared to that of the reference case, with particular attention being placed on the formation of the TEVs. Presentation of vorticity contour plots is limited to the reference and the quick-pitch A and C cases as these are representative of the three different types of TEVs encountered in this experiment. Fig. 7.3 shows the dimensionless vorticity contours of the flow field at $t/T = 0.417$ and at $t/T = 0.5$ for the reference, quick-pitch A and C cases. The flow moves from left to right and the airfoil translates downwards until it reaches the bottom-dead-center position at $t/T = 0.5$. Dark regions denote high absolute values of vorticity, whereby the positive (clockwise LEV) and negative (counter-clockwise TEV) regions are separated by white areas of near-zero vorticity. The area underneath the airfoil is masked due to shadows and reflections from the laser light sheet.

First the reference case without the quick-pitch motion is examined. At $t/T = 0.417$ the LEV has developed and its size is on the order of the chord length. At this phase the LEV passes over the trailing edge and the TEV is formed, as can be seen directly behind the trailing edge in Fig. 7.3(a). Here the TEV is the most concentrated of all cases. By $t/T = 0.5$ the TEV and LEV have formed the mushroom-wake structure, which then convects downstream. At $t/T = 0.5$ the TEV is found to have grown significantly in size and has convected half a chord length downstream from the trailing-edge, which represents a convection velocity of less than half the free-stream velocity.

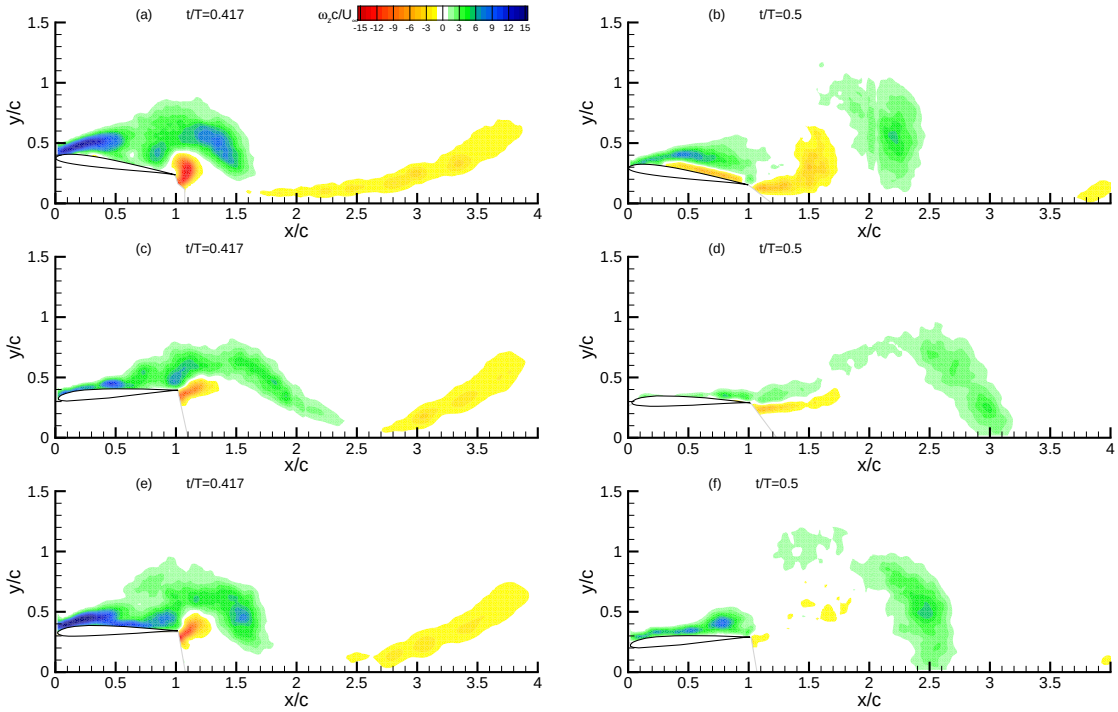

Figure 7.3: Plots of dimensionless vorticity showing the TEV formation one phase before bottom dead center ($t/T = 0.417$) and at bottom dead center ($t/T = 0.5$) for the reference (a)-(b), quick-pitch A (c)-(d) and quick-pitch C (e)-(f) cases.

When comparing the TEVs of the quick-pitch and reference cases with one another, major differences become apparent. Unlike the reference case, the airfoil for the quick-pitch A case is in the fully pitched-down position at $t/T = 0.417$. The first significant difference for this case is that the vortex structure at the trailing edge is much more *sheet-like*, reminiscent of a shear layer and less so of the well-defined vortical structure found for the reference case. This is a result of the early pronation, which prevents the formation of the TEV. Major differences between the reference and the quick-pitch C cases have also been identified. The flow field for the quick-pitch C case has similarities with both the reference and quick-pitch A cases. At $t/T = 0.417$ the airfoil is still pronating and a TEV is found at the trailing edge, similar to that of the reference case. In the next time step though, at $t/T = 0.5$, the TEV is significantly dissipated, which can be attributed to the interactions between the vortex and the trailing edge during the pronation.

In order to further understand the TEV development one must also consider the LEV, as the two are invariably linked to one another through Kelvin's law (Eq. 6.5). Despite the fact that the bound vortex cannot be measured in this study, a strong correlation between the circulation shed from the leading and trailing edges has been observed in Figs. 7.3(a), (c) and (e). At $t/T = 0.417$ the reference case has the strongest leading-edge shear layer and therefore also the strongest trailing-edge shear layer. Conversely for the quick-pitch A case, both the weakest leading- and trailing-edge shear layers are

found.

The phases where the LEV convects over the airfoil are the most important for lift production. In Fig. 7.4 the vorticity distribution for the LEV is shown at $t/T = 0.333$ for the various cases. For the reference case the LEV spans from the leading-edge shear layer back towards the trailing edge. A similar vortex is found for the quick-pitch C case, as the airfoil has not yet begun to pronate. For the quick-pitch A case minor differences are observed, which can be attributed to the early pronation of the airfoil. These differences include small structures inside the LEV, as well a downstream shift of the vortex position. Apart from these minor differences, however, the LEV size and strength is by and large the same as for the reference case. When returning to Fig. 7.3 one time step later at $t/T = 0.417$, it can be clearly seen that the pronation plays a dominant role on the LEV. However, it is difficult to make any quantitative comparison based on the vorticity distributions alone.

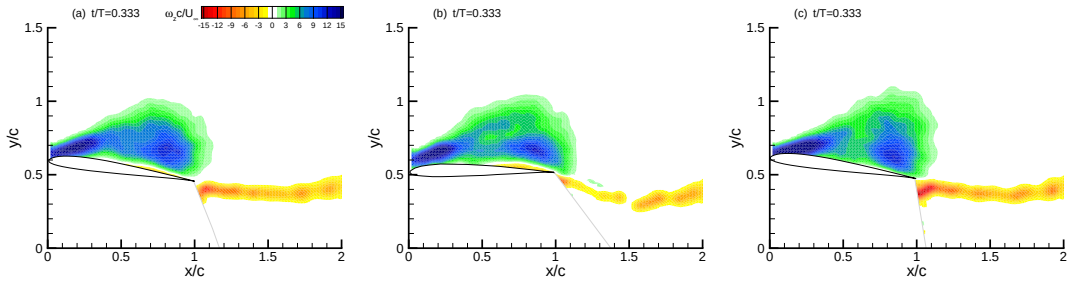

Figure 7.4: Plots of dimensionless vorticity showing the LEV formation at $t/T = 0.333$ for the reference (a), quick-pitch A (b) and quick-pitch C (c) cases.

7.2.2 Circulation

In order to compare the LEV strengths, the dimensionless circulation was calculated from the vorticity field using Stokes' theorem (Eq. 3.2). The dimensionless circulation curves for both the LEVs and TEVs are presented in Fig. 7.5(a) and a close-up of the TEV circulation is presented in Fig. 7.5(b). It can be seen that for all cases the LEV reaches its maximum strength just before pinching-off from the leading-edge shear layer, as discussed in section 6.3.1. The subsequent rapid decrease in out-of-plane vorticity, and therefore circulation, can be attributed to three-dimensional vortex breakdown associated with such massive separations. For the reference case the LEV circulation grows linearly until $t/T = 0.333$ at which point the LEV reaches the trailing edge. In comparison to the reference case, the early-pitching case (quick-pitch A) shows a light reduction in the LEV growth rate between the beginning of the quick-pitch motion at $t/T = 0.275$ and the maximum LEV strength at $t/T = 0.333$. Although the pronation begins at $t/T = 0.275$, a return to the static-stall angle is not reached until after the maximum LEV strength is achieved. At $t/T = 0.417$ the LEV convects into the wake and the lift augmentation drops. Therefore a reduction in LEV strength during this latter stage of the downstroke is not so detrimental to performance. Conversely for the late pitching cases (quick-pitch B, C and D), the maximum LEV circulation is somewhat higher. However, the general shapes of these LEV circulation curves are nearly identical to the reference case and are only affected by the state of the boundary layer at the beginning of the downstroke. An exception to this is the quick-pitch A case, which has a somewhat different shape than the other cases. Its LEV circulation curve shares more similarities with the reference case than with the other quick-pitch cases (B-D), which show effectively no variation amongst themselves. The similarity between these later cases indicates that after approximately

t/T=0.3 the dynamic-stall process becomes rather insensitive to the timing of the quick-pitch motion. When examining the LEV circulation development in Fig. 7.5(a), one can observe that for all quick-pitch cases the LEV begins to form somewhat earlier during the downstroke and reaches a greater maximum value. This variation in LEV formation is attributed to a more quasi-steady boundary layer at the top-dead-center position as a result of earlier flow reattachment during the upstroke. Such history effects have previously been discussed in section 6.3.1.

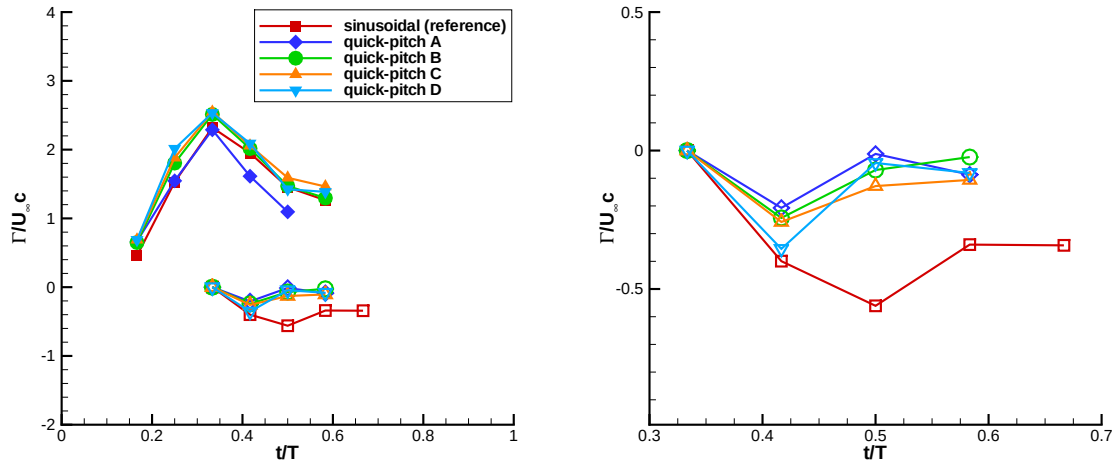

Figure 7.5: Development of LEV (solid) and TEV (hollow) circulation as a function of period (a), and a close-up of the TEV circulation growth (b).

Insight into the reduction of TEV strength can be obtained from the plot of dimensionless circulation in Fig. 7.5. Circulation is used in order to perform a quantitative comparison of the TEV strength between the reference and quick-pitch cases. When examining the counter-clockwise (negative) circulation in Fig. 7.5(b), it is evident that for all quick-pitch cases the TEV is significantly diminished. The maximum circulation has moved forward by one phase in all quick-pitch cases from $t/T = 0.5$ to $t/T = 0.417$. Moreover the new maxima in TEV circulation at $t/T = 0.417$ are lower than the corresponding value for the reference case. For the quick-pitch C case it is even less than half the maximum circulation of the reference case. At $t/T = 0.5$ the TEV circulation for all quick-pitch cases is less than a quarter of the peak reference TEV circulation. Table 7.2 shows the dimensionless TEV circulation values for the relevant phases from $t/T = 0.417$ to 0.583. After summing up the circulation for the three phases when the TEV is present at the trailing edge - where the influence on performance is greatest - it becomes clear that the TEV circulation has been reduced in all cases by at least 60%.

7.2.3 Statistical Analysis of TEV

Since ensemble averaging has the potential of *hiding* vortex structures due to a cycle-to-cycle variation in the vortex positions, it was deemed prudent to examine the TEVs of each individual cycle separately. In order to ensure that the differences between the reference and quick-pitch TEVs computed from the ensemble-averaged flow fields are representative of the individual cycles, a statistical analysis of the TEV strength was performed. Instead of calculating the vortex strength from the ensemble-averaged flow field, the circulation was calculated for each of the 100 individual cycles without the

use of a threshold. Since many small vortical structures due to the inherent turbulent breakdown are measured, positive values are at times obtained. Histograms of TEV circulation for the reference and quick-pitch C cases at $t/T = 0.5$ are presented in Fig 7.6. This time step (at the bottom of the stroke) was selected since it demonstrates the largest variation within the cycle, and offers some insight into the stochastic nature of the vortex breakdown. The mean of the individual TEV circulation and its corresponding standard deviation are shown above the TEV circulation distributions. The mean dimensionless circulation for the reference case is equal to -0.46, which is significantly larger than the value of -0.08 for the quick-pitch C case. Furthermore, the quick-pitch C case is more repeatable than the reference case, as can be seen when comparing their respective standard deviations. Moreover the difference between the mean circulation of the two cases is larger than the standard deviation of the reference case. Therefore it can be concluded that the ensemble-averaged field is representative of the individual cycles and the reduction in TEV circulation occurs not only for an ensemble-averaged data set but for individual cycles as well.

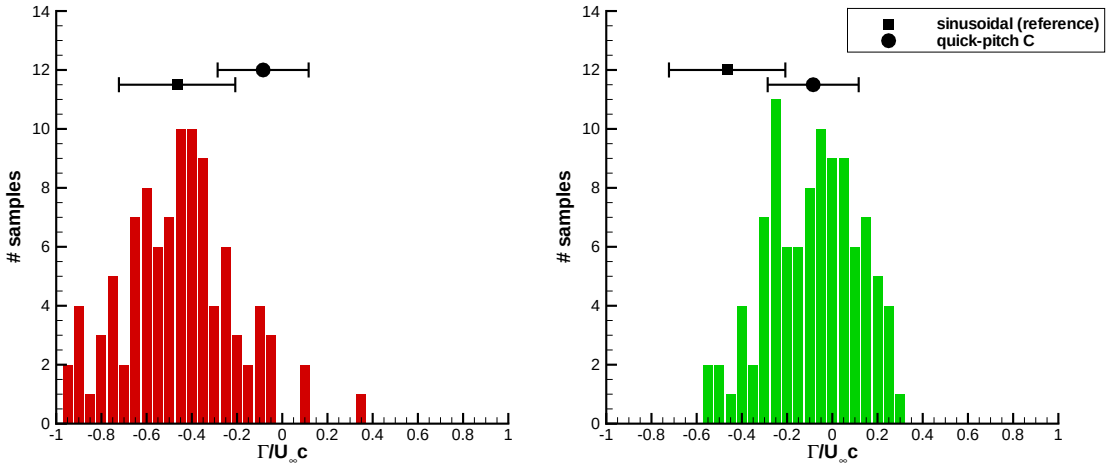

(a) (b)

Figure 7.6: Histograms of dimensionless circulation for the reference case (a) and the quick-pitch C case (b); mean and standard deviations for both cases shown above for reference.

Table 7.2: Dimensionless circulation of the TEV at various points in the cycle.

case	reference	quick-pitch A	quick-pitch B	quick-pitch C	quick-pitch D
$t/T = 0.417$	-0.400	-0.206	-0.243	-0.257	-0.354
$t/T = 0.500$	-0.561	-0.001	-0.070	-0.128	-0.045
$t/T = 0.583$	-0.340	-0.087	-0.024	-0.106	-0.081
$\sum$	-1.301	-0.294	-0.337	-0.491	-0.480
%	100%	23%	25%	38%	37%

7.2.4 Reattachment

In order to gain insight into the reattachment process, contour plots of dimensionless stream-wise velocity are presented in Fig. 7.7. For the reference case the separation opens at $t/T = 0.333$ as the outer regions of the LEV reach the trailing edge. After the static-stall angle is crossed just before the bottom-dead-center position, the flow begins to reattach. At $t/T = 0.5$ and $t/T = 0.583$ the flow at the leading edge of the airfoil is attached and the reattachment process moves towards the trailing edge, culminating in a fully-attached flow over the airfoil at $t/T = 0.75$.

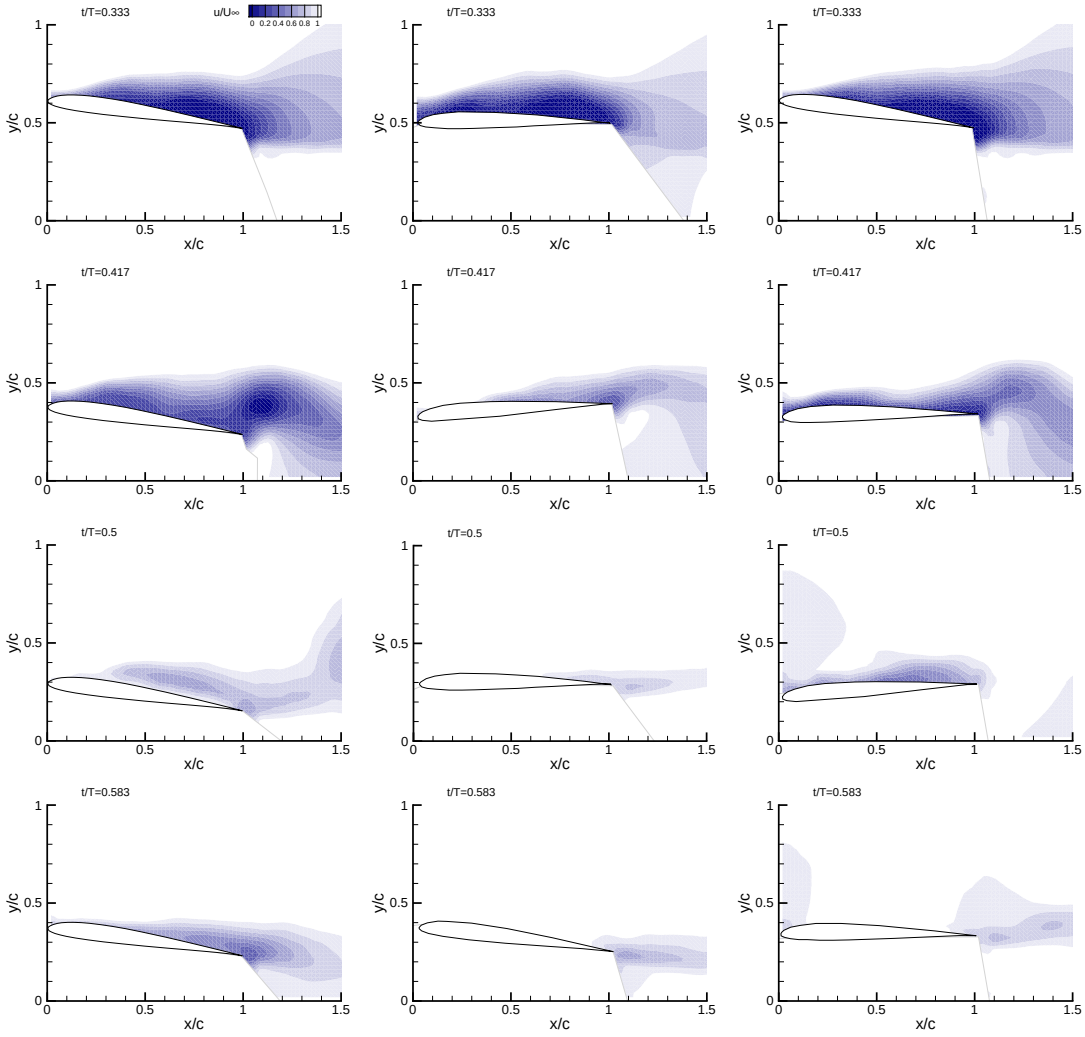

Figure 7.7: Contour plots of dimensionless stream-wise velocity (u/U_∞) for the phases $t/T = 0.333$, $t/T = 0.417$, $t/T = 0.5$ and $t/T = 0.667$; reference case (left column), quick-pitch A (center column) and quick-pitch C (right column).

The velocity contours for the quick-pitch cases were found to differ from the reference case after sharing a similar stalled condition at $t/T = 0.333$. In particular, the quick-pitch C and reference cases are nearly identical to one another at this point in time. One phase later, at $t/T = 0.417$, the first significant differences in the flow separation become apparent. Here the reference and quick-pitch C cases share a similar saddle shape. In contrast to both these cases, the quick-pitch A case already has flow reattachment at the leading edge. The differences encountered at $t/T = 0.417$ are amplified in the remaining

time steps, resulting in attached flow at $t/T = 0.5$ and $t/T = 0.583$ for the quick-pitch cases A and C, respectively. Therefore it can be concluded that the quick-pitch cases achieve attached flow two to three time steps ($0.167 < \Delta t/T < 0.25$) before the reference case. Hence, the duration of the reattachment process is more than one time step shorter for the quick-pitch cases. These differences can be attributed to two effects: The first effect being the timing of the pronation and therefore the crossing of the static-stall angle earlier in the cycle, thus initiating the convective mechanism, and the second effect being the high rate of pitch that accelerates the boundary-layer re-establishment, as demonstrated by Green and Galbraith (1995) and Schreck et al (1996). In this study, however, the time resolution does not allow for a distinguishment between these two effects on the reattachment process.

7.3 Summary

The manipulation of TEVs for a pitching and plunging airfoil has been investigated using PIV. Various quick-pitch motions were developed and tested in comparison to a pure-plunge reference case, resulting in two distinct flow patterns where the TEV was either reduced in strength or even completely avoided. The latter, represented by quick-pitch A, prevents the formation of a TEV by pitching the airfoil down before the TEV can even begin to form. For the case of TEV circulation reduction, represented by quick-pitch C, the pronation takes place later. Here a TEV begins to form but is quickly dissipated as soon as the airfoil pitches down. All quick-pitch cases demonstrated a reduction of TEV circulation of at least 60%. It has been shown that airfoil kinematics can be used to reduce the negative aspects associated with the dynamic-stall process without infringing upon the lift-augmenting LEV over the airfoil. Flow separation was also investigated and it was found that quick-pitch leads to earlier flow reattachment. This earlier start and shorter duration of the flow reattachment process has the potential to reduce drag and the amount of hysteresis, which can increase the mean lift over the cycle.